Velocity contrast along the Calaveras fault from analysis of fault zone head waves generated by repeating earthquakes

Peng Zhao[1] and Zhigang Peng[1]

Received 29 August 2007; revised 1 November 2007; accepted 20 November 2007; published 1 January 2008.

[1] We systematically investigate the velocity contrast along the Calaveras fault that ruptured during the 1984 Morgan Hill earthquake using fault zone head waves (FZHW) that refract along the fault interface. We stack waveforms in 353 sets of repeating clusters, and align the peaks or troughs of the direct *P* waves assuming right-lateral strike-slip focal mechanisms. The obtained velocity contrasts are 2–3% and 12–14% NW and SE of station CCO, respectively. The FZHW and the fault plane outlined by the relocated seismicity SE of CCO are more complicated than those NW of CCO. The results can be explained by a relatively simple and sharp fault interface in the NW, and a complicated fault structure with a presence of a low-velocity zone in the SE. The along-strike variations in the strength of the velocity contrast are consistent with surface geological mapping and recent 3D tomography studies in this region. **Citation:** Zhao, P., and Z. Peng (2008), Velocity contrast along the Calaveras fault from analysis of fault zone head waves generated by repeating earthquakes, *Geophys. Res. Lett.*, *35*, L01303, doi:10.1029/2007GL031810.

1. Introduction

[2] Large crustal faults typically juxtapose rocks with different elastic properties, resulting in well-defined bimaterial interfaces. An accurate determination of the fault interface properties at seismogenic depth can be important for various aspects of earthquakes and fault dynamics [e.g., *Ben-Zion*, 2001], and better quantification of earthquake locations and focal mechanisms [e.g., *Hardebeck et al.*, 2007].

[3] A sharp material contrast across a fault interface can generate fault zone head waves (FZHW) that spend a large portion of the propagation paths refracting along the bimaterial interface [*Ben-Zion*, 1989, 1990; *Ben-Zion and Aki*, 1990]. These waves are characterized by emergent waveforms with opposite motion polarities to those of the direct *P* waves, and are recorded only by stations on the slow side of the fault [*Ben-Zion and Malin*, 1991]. FZHW provide a high-resolution tool for detecting the existence of sharp bimaterial interface, and imaging their seismic properties at seismogenic depth.

[4] So far, FZHW were only observed along the main San Andreas fault (SAF) at Parkfield [*Ben-Zion and Malin*, 1991], and south of Hollister [*McGuire and Ben-Zion*, 2005; *Lewis et al.*, 2007]. In this work, we show clear evidence of FZHW along the central portion of the Calaveras fault that ruptured during the 1984 M6.2 Morgan Hill earthquake (Figure 1), and use them to quantify the along-strike variations of the fault interface properties. This section of the fault juxtaposes the Franciscan complex (fast) in the NE side and a sequence of marine sediments (slow) in the SW side deposited mostly during the Cretaceous [*Page*, 1984]. Seismic tomography studies in this region have found 6–14% of *P*-wave velocity contrast that extends to at least 5 km depth [*Michael*, 1988; *Thurber et al.*, 2007], consistent with the geological observations.

[5] More than 40% of the seismicity in the aftershock zone of the Morgan Hill mainshock belongs to repeating earthquakes [*Peng et al.*, 2005]. Since repeating earthquakes rupture almost the same fault patch, they generate nearly identical waveforms. We take advantage of the abundant repeating earthquakes in the study region, and stack waveforms in each repeating cluster to enhance the signal-noise ratio (SNR) and the confidence levels of the FZHW identification. In the next section, we briefly describe the method to identify repeating clusters. In section 3, we present the detailed procedures of stacking and aligning waveforms. The results are shown in section 4 and are discussed in section 5.

2. Repeating Earthquake Identification

[6] We identify repeating clusters in the study region using 7857 earthquakes relocated by *Schaff et al.* [2002]. The detailed procedure is as follows. We first compute the inter-event distances for all earthquake pairs along and perpendicular to the fault strike of 146°. The source radius of each event is estimated from its catalog magnitude, based on a moment-magnitude relationship [*Abercrombie*, 1996] and a circular crack model [*Eshelby*, 1957] with a nominal 3-MPa stress drop. Two events are considered as a pair if their inter-event distance along the fault strike is less than the source radius of the larger event. Next, we organize the event pairs into clusters using the equivalency class (EC) algorithm [*Press et al.*, 1986]. We do not include those events with inter-event distances perpendicular to the fault strike larger than the source radius. Using the above criteria, we identify a total of 353 repeating clusters, with at least five events in each cluster.

[7] We note that the number of identified repeating clusters depends on the assumed model parameters (e.g., the constant stress drop value and the circular crack model) and other selection criteria. However, since our main goal of using repeating clusters is to stack waveforms that are highly similar to enhance the SNR and confidence levels of FZHW identification, using slightly different parameters

[1]School of Earth and Atmospheric Sciences, Georgia Institute of Technology, Atlanta, Georgia, USA.

0094-8276/08/2007GL031810$05.00

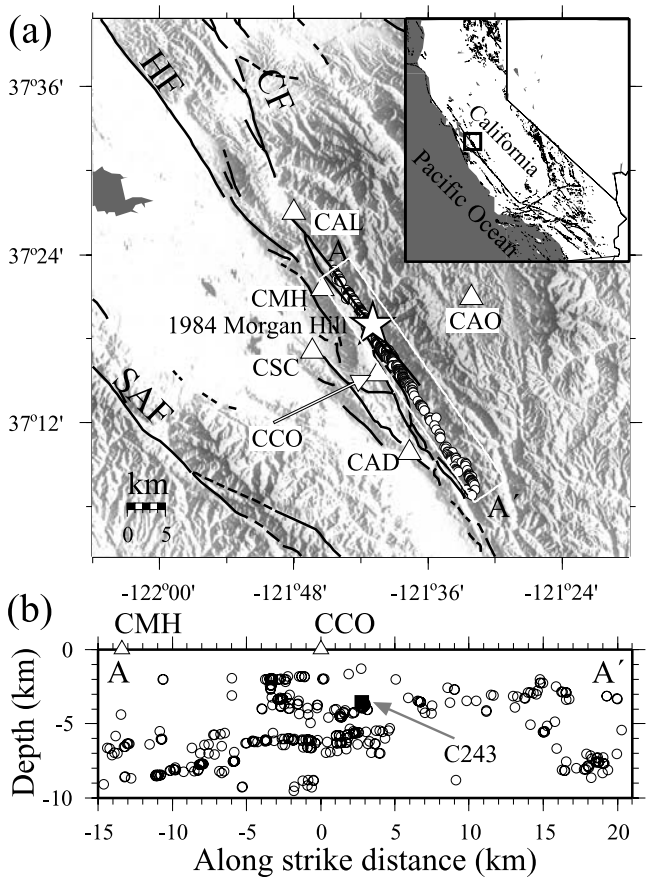

Figure 1. (a) Location of the central section of the Calaveras fault in California. Dark lines denote nearby faults. The circles denote the 353 repeating clusters employed in this study. The star marks the epicentral location of the 1984 Morgan Hill mainshock. Triangles denote six stations in the NCSN. Shaded background indicates topography with white being low and dark being high. The inset shows the map of California with the box corresponding to the study area. SAF, San Andreas fault; CF, Calaveras fault; HF, Hayward fault. (b) The centroid locations of 353 repeating clusters in the cross-section map along the Calaveras fault (146° strike). Waveforms generated by events in cluster C243 (the sold black square) are shown in Figure S1.

will not change the overall features of the waveform stacks and our main conclusions.

3. Waveform Stacking and Alignment

[8] This study employs seismic data recorded by surface stations in the Northern California Seismic Network (NCSN). Each station has a high-gain, short-period, vertical-component sensor, and records at 100 samples/s. The FZHW are the first arriving phases at locations on the slower block with normal distance to the fault [*Ben-Zion*, 1989] less than a critical distance x_c given by

$$x_c = r \cdot \tan\left[\cos^{-1}\left(\alpha_2/\alpha_1\right)\right], \quad (1)$$

where r is the total propagation distance along the fault (both along-strike and up-dip direction) and α_2 and α_1 are the average P wave velocities of the slower and faster media, respectively. Using a nominal distance r of 10 km, and an average velocity contrast of 10% from previous tomography studies [*Michael*, 1988; *Thurber et al.*, 2007], the critical distance x_c is about 5 km. For the six NCSN stations that are within 15 km of the Calaveras fault (Figure 1), only stations CCO and CMH are within the critical distances on the slow side (SW) of the fault to record FZHW as the first arriving phases.

[9] Prior to the analysis, we remove the mean and trend of each trace, and apply a 4-pole two-way Butterworth high-pass filter with a corner at 1 Hz to suppress long-period noise. Next, we select a reference trace that has the highest similarity with others in each repeating cluster, and remove those traces with cross-correlation coefficient to the reference smaller than 0.8, or the SNR smaller than 2. We then normalize the amplitude of each trace by its maximum value, and linearly sum all the traces after aligning with the reference trace to obtain a single stack in each cluster (Figure S1 of the auxiliary material).[1]

[10] Next, we align the peaks or troughs of the stacked direct P waves (Figure 2), assuming right-lateral fault mechanisms for all clusters. This is justified by the fact that the majority of the microseismicity in the Morgan Hill rupture zone have strike-slip focal mechanisms on near-vertical planes [*Michael*, 1988; *Schaff et al.*, 2002]. We also use the first motion polarity from other NCSN stations to confirm the radiation patterns. After aligning the P waves, we manually pick the arrival times of the FZHW by comparing with the waveform stacks of nearby clusters.

[11] After picking of the FZHW phases, we obtain a total of 308 (2181 events) and 312 (2126 events) stacked traces for stations CCO and CMH, respectively. We dropped 45 traces for station CCO, and 41 traces for station CMH, because the data are severely clipped, or the stations are outside the critical distances x_c for some nearby events. We also checked the waveforms and found no clear FZHW recorded at other four stations, CAO, CAL, CAD, and CSC, since they are either on the fast side (SE), or beyond the critical distance to record FZHW as first arrivals.

4. Variations of Velocity Contrast Along Strike and Depth

[12] The stacked waveforms and FZHW arrivals are shown in Figure 2 for stations CCO and CMH. Clear head waves are recorded at both stations with motion polarities opposite to those of the direct P waves. The time difference (Δt) between the FZHW and the direct P waves, or moveout, increases with distance along the fault interface r, indicating the existence of a sharp velocity contrast in this region. We find that the FZHW moveout SE of station CCO has a larger slope than that to the NW, suggesting a possible change of velocity contrast along the fault strike. In addition, the moveout to the NW follows a linear trend, and the head wave signals are relatively simple. In comparison, the moveout to the SE is more scattered, and the head wave

[1] Auxiliary materials are available in the HTML. doi:10.1029/2007GL031810.

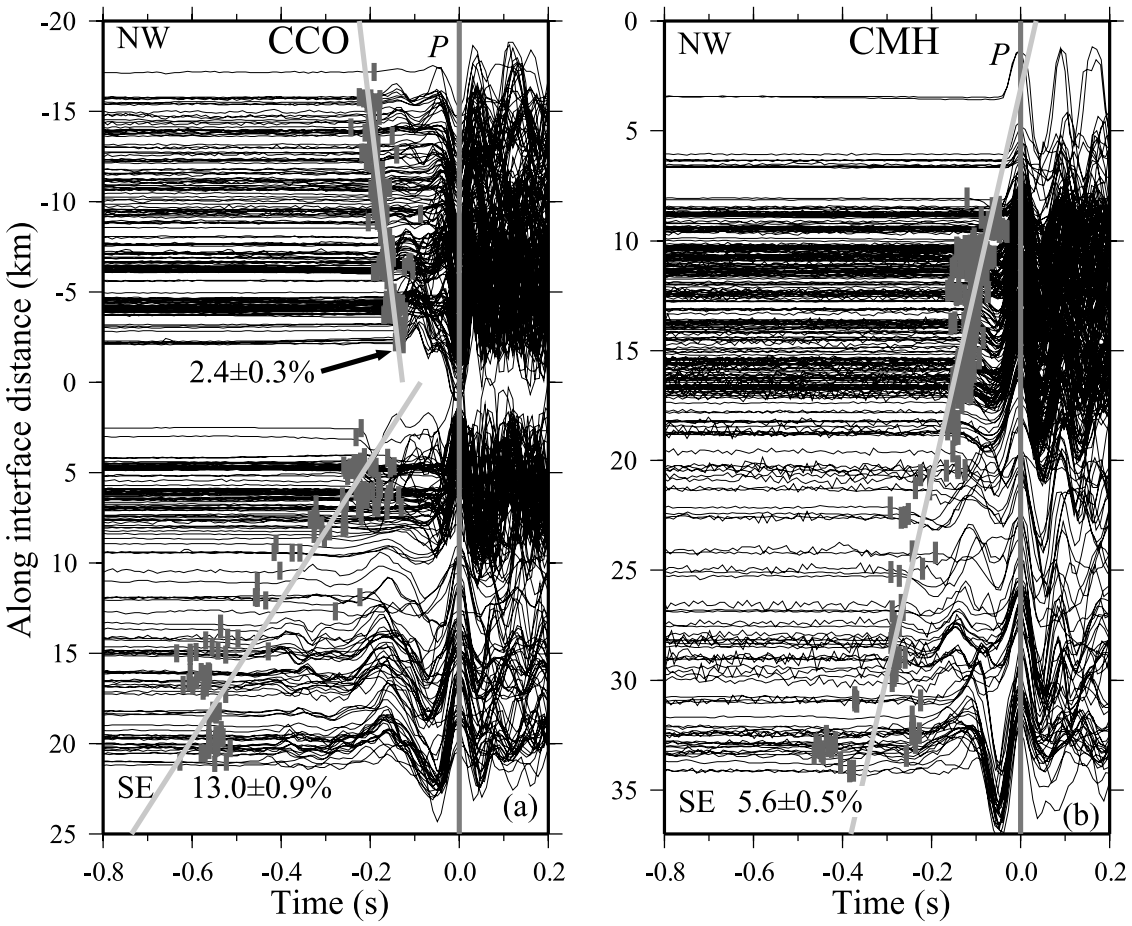

Figure 2. (a) Stacked traces at station CCO showing the moveout of the FZHW. The vertical-axis is the along fault-interface distance between the centroid location of each cluster and station CCO along the Calaveras fault (146° strike). The *P* arrivals are aligned with their peaks or troughs depending on the relative locations of clusters to station CCO, assuming right-lateral strike-slip focal mechanisms. Short vertical bars mark the fault zone head wave arrivals. The gray lines mark the slope of moveout by the least-squares fitting of the head wave picks. The corresponding velocity contrasts with an average *P* wave velocity of 5 km/s are marked. The error is the 95% confidence interval from 5000 bootstraps. (b) Stacked traces at station CMH showing the moveout of the head waves. All symbols are the same as in Figure 2a.

signals are more complicated. The moveout and head wave signals at station CMH also show similar changes at a distance of ~20 km (near station CCO), consistent with the patterns observed at CCO.

[13] The *P* wave velocity contrast $\Delta\alpha$ can be estimated from the slope of the differential arrival time Δt and the along-interface distance r as [*Ben-Zion and Malin*, 1991]

$$\Delta\alpha = \frac{\Delta t}{r} \cdot \alpha^2 \tag{2}$$

where α is the average *P* wave velocity. Assuming α = 5 km/s based on the average velocity model used by *Schaff et al.* [2002], we obtain from least-squares fitting average velocity contrasts $\Delta\alpha/\alpha$ to the NW and SE of CCO of 2.4 ± 0.3% and 13.0 ± 0.9%, respectively. The $\Delta\alpha/\alpha$ value is 5.6 ± 0.5% for station CMH. If we separate the data for CMH for $r \leq 20$ km and $r > 20$ km, the obtained $\Delta\alpha/\alpha$ are 3.3 ± 0.5% and 6.3 ± 2.0%, respectively. The error is the 95% confidence interval from 5000 bootstraps.

[14] To quantify the depth dependence of the velocity contrasts, we divide the clusters according to their average hypocentral depths as shallow (depth $\leq$ 5 km) and deep (depth > 5 km) groups, and fit the data points in each group separately (Figure 3). The velocity contrasts for shallow clusters to the NW and SE of CCO are slightly larger than that for the deep clusters, while the pattern is opposite for station CMH. However, the differences for shallow and deep groups are probably not significant due to scatters in the measurements and overlapping confidence intervals. So the dominant variations of the imaged velocity contrasts are along-strike.

5. Discussion

[15] The existence of the FZHW indicates a sharp material interface along the Calaveras fault. The time difference

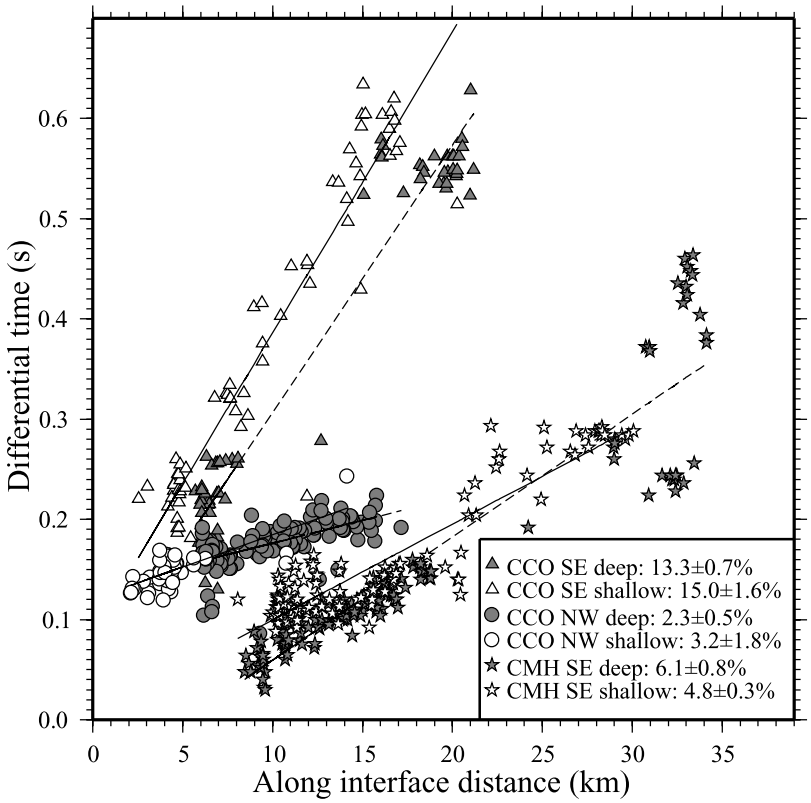

Figure 3. Differential arrival times between FZHW and direct *P* waves versus the along fault-interface distances for stations CCO and CMH. The data points are divided into shallow (depth $\leq$ 5 km) and deep (depth > 5 km) groups. The solid and dashed lines are least-squares fittings for shallow and deep groups, respectively. The velocity contrasts for different groups are shown on the bottom right.

Δt between the FZHW and the direct *P* waves can be used to document the along-strike and down-dip variations of the strength of the material contrast. Our results are summarized in Figure 4 in map and cross-section views. The velocity contrast NW of station CCO is 2–3%, and the head wave signals are relatively simple. This is consistent with a well-defined fault structure outlined by the microseismicity [*Schaff et al.*, 2002], indicating a simple and sharp fault interface that extends to the bottom of the seismogenic depth in that segment. In comparison, the velocity contrast SE of station CCO is 12–14%, and the head wave signals are complicated with many phases between the FZHW and the direct *P* waves. The existence of such complicated FZ phases suggests a thick transition zone between the two sides of the fault [*McGuire and Ben-Zion*, 2005]. In addition, the seismicity in the SE is relatively diffuse, and the surface expression of the Calaveras fault does not coincide with the fault interface inferred from the earthquake locations [*Michael*, 1988; *Schaff et al.*, 2002]. These evidence suggest the existence of a low-velocity zone SE of station CCO that extends to the depth of a few kilometers in the SW (slow) side of the fault.

[16] The obtained variations in the strength of the velocity contrasts along the Calaveras fault using FZHW are consistent with surface geology and recent 3D tomography studies in this region. A surface geological map shows an apparent change of rock types along the Calaveras fault near station CCO [*Page*, 1984]. The surface trace cuts through the Franciscan Complex NE of CCO, resulting in a well-defined fault interface and a small velocity contrast. In comparison, the fault SE of CCO juxtaposes a low-velocity marine sedimentary rock in the SW side and the faster Franciscan Complex in the NE side. Several 3D tomography studies also indicate an apparent low-velocity body south of CCO, down to a depth of ~5 km [*Michael*, 1988; *Thurber et al.*, 2007]. This low-velocity body is also inferred from the head wave analysis in this study, and is likely corresponding to the surface expression of the sedimentary layer in the SW side of the Calaveras fault.

[17] A detailed 3D high-resolution image of the FZ properties in this region can be obtained by traveltime inversions and waveform modeling of the FZHW and direct *P* waves [e.g., *McGuire and Ben-Zion*, 2005; *Lewis et al.*, 2007]. This will be pursued in a follow up study. Our results demonstrate that stacking waveforms generated by repeating clusters provides an effective tool for increasing the SNR and confidence levels of FZHW

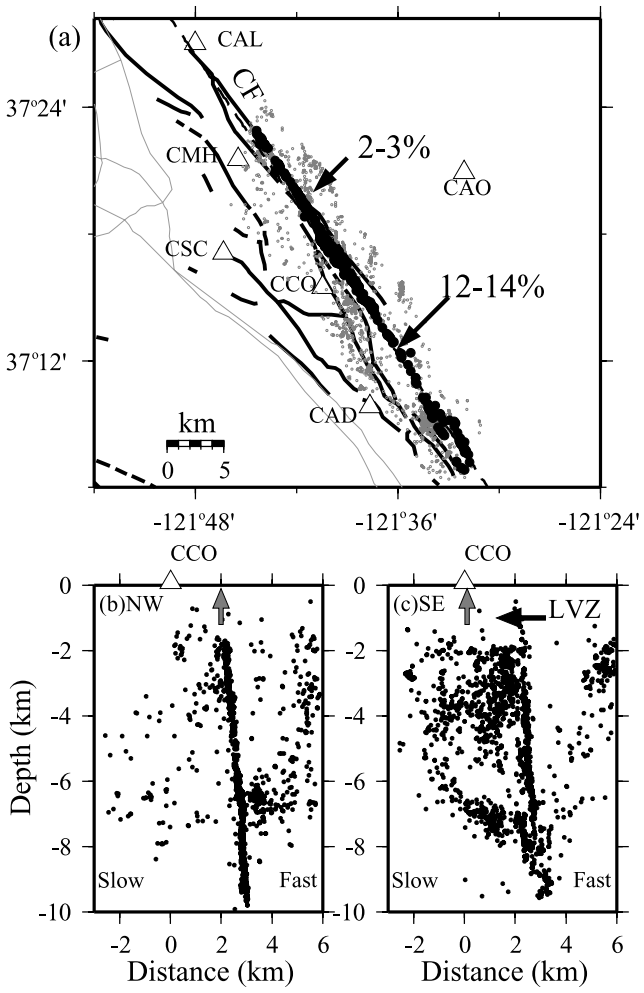

Figure 4. Schematic summary of the results from the traveltime analysis of FZHW at stations CCO and CMH. (a) Map view of the Calaveras fault (CF) with the entire relocated seismicity (grey dots) from *Schaff et al.* [2002] and the 353 repeating clusters employed in this study (solid black circles). The estimated velocity contrasts in the NW and SE sections are labeled with the arrows. Dark lines denote nearby faults. (b) Cross-section view perpendicular to the strike of the fault (146°) with projection of the all earthquakes (black dots) NW of station CCO. The triangle and grey arrow mark the projected locations of CCO and the surface trace of the Calaveras fault. (c) Cross-section view for all earthquakes SE of station CCO. The inferred low-velocity zone (LVZ) is marked by a vertical black arrow.

identification, while reducing the total numbers of analyzed waveforms from several thousands to a manageable number of several hundreds. The sensitivity of FZHW to the changes of bimaterial interface properties along the fault strike indicates that head waves provide a high-resolution tool for imaging fault zone properties at seismogenic depth.

[18] **Acknowledgments.** We thank the Northern California Earthquake Data Center for managing the waveform database of the NCSN, and David Schaff for making his relocated catalog available. The manuscript benefited from useful comments by Yehuda Ben-Zion, Michael Lewis, Andy Michael, Justin Rubinstein, John Vidale, and an anonymous reviewer.

References

Abercrombie, R. E. (1996), The magnitude-frequency distribution of earthquakes recorded with deep seismometers at Cajon Pass, southern California, *Tectonophysics*, *261*, 1–7.

Ben-Zion, Y. (1989), The response of two joined quarter spaces to SH line sources located at the material discontinuity interface, *Geophys. J. Int.*, *98*, 213–222.

Ben-Zion, Y. (1990), The response of two half spaces to point dislocations at the material interface, *Geophys. J. Int.*, *101*, 507–528.

Ben-Zion, Y. (2001), Dynamic ruptures in recent models of earthquake faults, *J. Mech. Phys. Solids*, *49*, 2209–2244.

Ben-Zion, Y., and K. Aki (1990), Seismic radiation from an SH line source in a laterally heterogeneous planar fault zone, *Bull. Seismol. Soc. Am.*, *80*, 971–994.

Ben-Zion, Y., and P. Malin (1991), San Andreas fault zone head waves near Parkfield, California, *Science*, *251*, 1592–1594.

Eshelby, J. D. (1957), The determination of the elastic field of an ellipsoidal inclusion and related problems, *Proc. R. Soc. London, Ser. A*, *241*, 76–396.

Hardebeck, J. L., A. J. Michael, and T. M. Brocher (2007), Seismic velocity structure and seismotectonics of the eastern San Francisco bay region, California, *Bull. Seismol. Soc. Am.*, *97*, 826–842, doi:10.1785/0120060032.

Lewis, M. A., and J. McGuire (2007), Imaging the deep structure of the San Andreas Fault south of Hollister with joint analysis of fault-zone head and direct P arrivals, *Geophys. J. Int.*, *169*, 1028–1042.

McGuire, J., and Y. Ben-Zion (2005), High-resolution imaging of the Bear Valley section of the San Andreas fault at seismogenic depths with fault-zone head waves and relocated seismicity, *Geophys. J. Int.*, *163*, 152–164.

Michael, A. (1988), Effects of three-dimensional velocity structure on the seismicity of the 1984 Morgan Hill. California, aftershock sequence, *Bull. Seismol. Soc. Am.*, *78*, 1199–1221.

Page, B. M. (1984), The Calaveras fault zone of California, an active plate boundary element, in *The 1984 Morgan Hill, California Earthquake*, *Spec. Publ.*, vol. 68, edited by J. H. Bennett and R. W. Sherburne, pp. 109–122, Calif. Div. of Mines and Geol., Sacramento.

Peng, Z., J. E. Vidale, C. Marone, and A. Rubin (2005), Systematic variations in recurrence interval and moment of repeating aftershocks, *Geophys. Res. Lett.*, *32*, L15301, doi:10.1029/2005GL022626.

Press, W., B. Flannery, S. Teukolsky, and W. Vetterling (1986), *Numerical Recipes*, Cambridge Univ. Press, Cambridge, U. K.

Schaff, D. P., G. H. R. Bokelmann, G. C. Beroza, F. Waldhauser, and W. L. Ellsworth (2002), High-resolution image of Calaveras Fault seismicity, *J. Geophys. Res.*, *107*(B9), 2186, doi:10.1029/2001JB000633.

Thurber, C. H., T. M. Brocher, H. Zhang, and V. E. Langenheim (2007), Three-dimensional *P* wave velocity model for the San Francisco Bay region, California, *J. Geophys. Res.*, *112*, B07313, doi:10.1029/2006JB004682.

Z. Peng and P. Zhao, School of Earth and Atmospheric Sciences, Georgia Institute of Technology, 311 Ferst Drive, Atlanta, GA 30332, USA. (pzhao@gatech.edu)

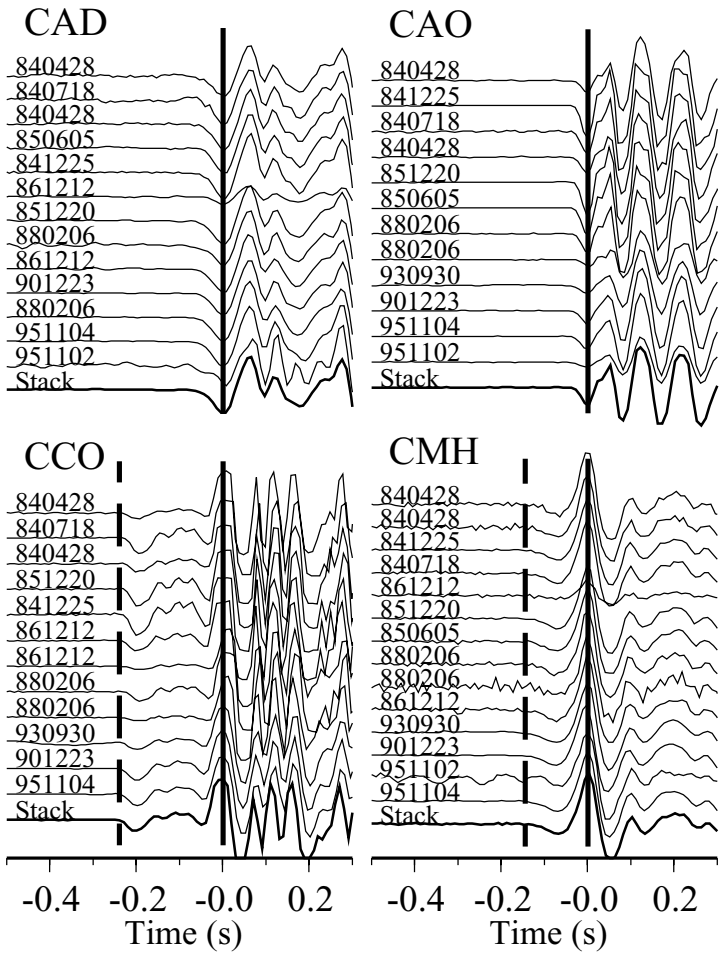

Figure S01. Vertical-component seismograms around the P arrivals generated by events in cluster C243 and recorded by four stations. The dashed and solid vertical lines mark the arrivals of FZHW and direct P waves, respectively. The bottom trace (thick line) is a simple stack of normalized individual traces at each station by aligning with the P waves. The occurrence time of each event (2 digit year, month and day) is shown on the left of each trace.

Auxiliary materials are available in the HTML. doi:10.1029/2007GL031810.